Journal of Biomechanical Science and Engineering

Vol. 2, No. 4, 2007

Stress Analysis of PS Type Knee Prostheses under Deep Flexion*

Mitsugu TODO**, Ryuji NAGAMINE*** and Shota YAMAGUCHI**

**Research Institute for Applied Mechanics, Kyushu University,
6-1 Kasuga-koen, Kasuga 816-8580, Japan
E-mail: todo@riam.kyushu-u.ac.jp
***Yoshizuka Hayashi Hospital,
7-6-29 Yoshizuka, Hakata, Fukuoka 812-0041, Japan

Abstract

3-D finite element models of two kinds of Stryker's PS type knee prostheses, Scorpio Superflex and NRG, were constructed using their CAD data with use of a nonlinear spring model and an analytical load data for deep squatting. Superflex model was formerly used in TKA, and NRG model is the latest version with a modified design of Post. Stress analysis was then performed by an explicit finite element method under continuous flexion motion from 0 to 135 degree. It was shown that only the condylar surfaces of the femoral component and the tibial insert contacted each other from 0 to 60 degree flexion for both the models, and the stress concentration in NRG was a little higher than that in Superflex. The simulation results also exhibited that severe stress concentration was generated at Post of the tibial UHMWPE insert due to Post/Cam contact. This kind of stress concentration may result in damage and failure of Post. It was shown that the design modification applied to NRG effectively reduced the stress concentration of Post.

Key words: Total Knee Arthroplasty, UHMWPE Insert, Deep Flexion, Finite Element Analysis

1. Introduction

Total knee arthroplasty, TKA, is applied to patients with severe osteoarthritis, and in general, QOL of the patients is dramatically improved after TKA. Although the function of knee prosthesis is being improved through design modification, there are still some demands for knee prosthesis such as higher durability of tibial insert and deeper flexion angle to fit Japanese life style, for example, 150 degree for kneeling on a tatami mat. It is therefore needed to understand the detail of movements of the knee after TKA, and such information should be reflected to the design of knee prosthesis. It is however very difficult to understand the detail of TKA knee motion because of its complex movements characterized as a combination of flexion, external and internal rotation and roll-back. Fatigue fracture and severe wear of tibial inserts are sometimes reported, and they are thought to be caused by the stress concentration under such complex knee motions.

PS type knee prosthesis is known to be used in a type of TKA where anterior and posterior cruciate ligaments are removed. PS type prosthesis is characterized by the existence of Post-Cam structure to stabilize the knee movement through the Post-Cam contact. In this type of prosthesis, failure and wear of Post of the tibial insert are important problems and therefore, there is a demand for understanding the stress state of the tibial insert during knee motion. Under such circumstances, three-dimensional finite element method (FEM) has been utilized to characterize the 3D stress state of knee prosthesis.

*Received 11 June, 2007 (No. 07-0250)
[DOI: 10.1299/jbse.2.237]

In the previous studies of FEM simulations of TKA, most of them were aimed to analyze stress states under walking conditions with shallow flexions [1,2-5,8], and a few attempts have been made to analyze stress state under deep flexion [9-11]. Morra and Greenwald performed a deep flexion analysis of TKA, however, their work was limited to a certain deep flexion angle under simple loading condition [9]. On the contrary, the author's group developed simplified 3D FEM models using CAD data of knee prosthesis clinically used, and investigated effects of deep knee flexion and internal rotation on the stress state of the tibial inserts [10,11]. In these studies, however, the movement of the tibial inserts of the FEM models was completely restricted and, for example, roll-back behavior in the PS type model was introduced compulsory by moving the femoral component [11].

The aim of the present study is therefore to reproduce more natural roll-back behavior using a simple FEM model of PS type knee prosthesis, and to characterize the stress states of two different types of PS type knee prostheses with different Post and Cam design under deep flexion. 3D FEM models of the knee prostheses were developed from their CAD data. Nonlinear spring model and load data for deep squatting were utilized to simulate more precise knee motion than the motion previously analyzed [11]. Effects of wide range of flexion on the stress state of the condylar surfaces and Post of the tibial inserts were then assessed using the analytical results, and the 1st and the 2nd were compared to characterize the effect of the design modification on reduction of stress concentration and improvement of flexion angle.

2. Development of Finite Element Models

In this study, two different types of PS type knee prosthesis, Stryker Scorpio Superflex and Scorpio NRG, were analyzed to examine the effects of the design difference on the stress distribution in the tibial inserts. Superflex is called the 1st model and NRG the 2nd model, thereafter. The 2nd model, which is clinically used currently, can be recognized as a modified version of the 1st model, and especially, the shape of Post and Cam were redesigned to reduce stress concentration. Post of the 2nd has more round shape than that of the 1st, and the contact surface area of Cam to Post was modified to be larger in the 2nd than in the 1st. 3D-FEA models of the 1st and the 2nd consisting of femoral component, tibial component and tibial insert were constructed from their CAD data obtained from the manufacturer. In this modeling, the tiny parts of the femoral component and the stem of the tibial components were removed prior to finite element meshing in order to avoid extremely small meshes and reduce the number of meshes. It is noted that those removed parts were carefully chosen so that the removal did not affect on the simulation results. The simplified models of the PS type prostheses are shown in Fig.1.

Finite element meshed models are shown in Fig.2. The numbers of the nodes and the elements are 21958 and 89322 for the 1st model and 28254 and 121604 for the 2nd model, respectively. The material constants used in the analysis are shown in Table 1. The tibial insert originally made from UHMWPE (Ultra High Molecular Weight Polyethylene) was assumed to be an elastic-plastic material and to follow the von Mises yield criterion. The nonlinear stress-strain relationship experimentally obtained is shown in Fig.3 [7]. The femoral component made from Co-Cr alloy and the tibial component made from Ti alloy are much stiffer than UHMWPE, and therefore, assumed to be rigid body in order to reduce computational time. The friction coefficient between the femoral component and the tibial insert was chosen to be 0.04 [5]. It was assumed that the back surface of the tibial insert was perfectly connected to the top surface of the tibial component and therefore, the both surfaces possessed the nodes in common.

In a PS type knee prosthesis attached in a real human knee, reaction and frictional force are generated on the condylar and Post surfaces during motions. In this TKA knee, these forces are balanced with the tensions of the soft tissues existing around the knee; as a result,

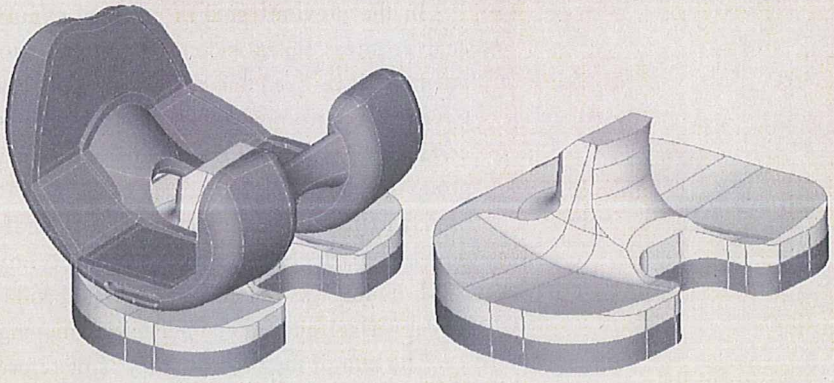

(a) 1st model

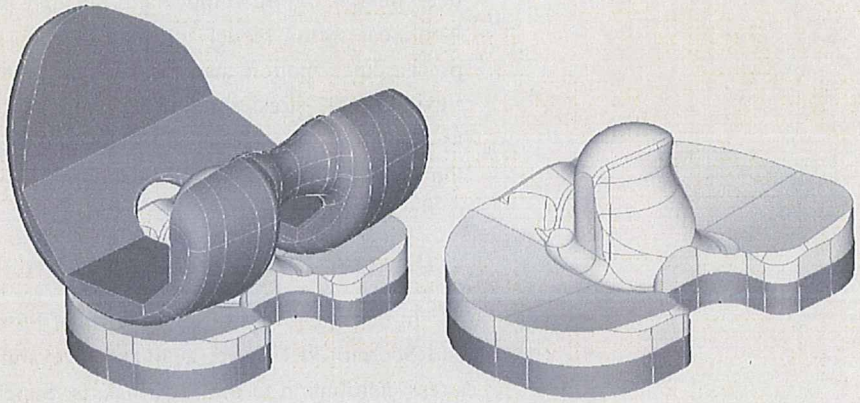

(2) 2nd model

Fig. 1 FEA models of two kinds of PS type knee prostheses.

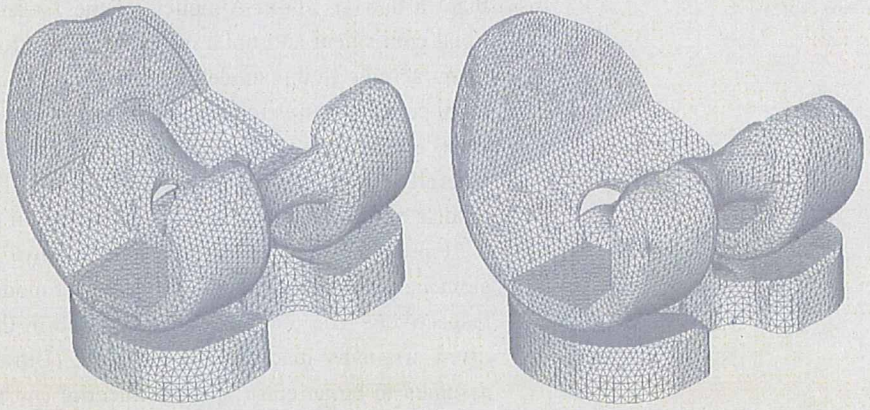

(1) 1st model (2) 2nd model

Fig. 2 FEA mesh models of PS type knee prostheses.

Table 1 Material constants for FEA.

Parts	Material	Density (kg/m^3)	E (MPa)	ν	σ_Y (MPa)
Tibial insert	UHMWPE	940	880	0.4	16

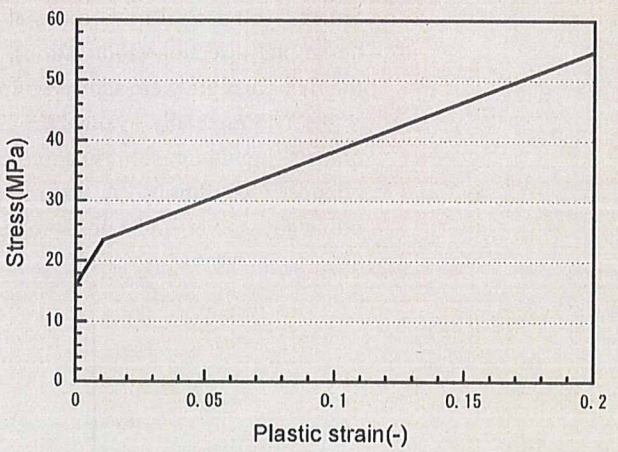

Fig. 3 Bi-linear relation of stress-plastic strain curve of UHMWPE.

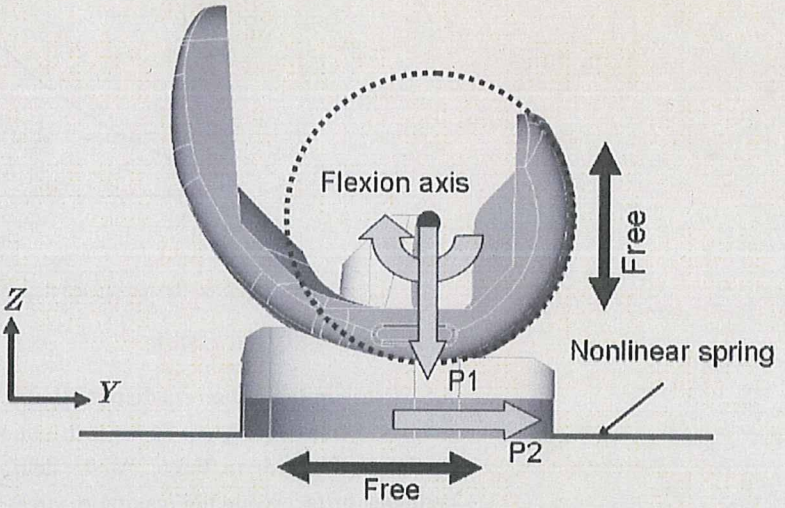

Fig. 4 Boundary conditions of the TKA model.

for example, roll-back motion occurs. In the present FEA models, a nonlinear spring model was utilized to express these motions in TKA [8]. Two spring elements were attached in the front of the tibial component and the two in the back as shown in Fig.4. The nonlinear force -displacement relation is given by

$$F = 0.18667d^2 + 1.3313d \quad (1)$$

where F and d are force and displacement, respectively. It is noted that this nonlinear relation was experimentally determined from a knee with removed anterior and posterior cruciate ligaments [8].

In the most of real knees, internal rotation tends to take place during flexion, and it was reported, for example, that 7 degree of internal rotation occurs at a deep flexion angle of about 135 degree [12]. In the present analysis, however, only flexional motion was considered in order to make the effect of the Post-Cam contact on the stress distribution clearer. The axis of flexion was assumed to be located in the center of the circle which coincides with the shape of the condylar surface of the femoral component (see Fig.4). For the femoral component, only the displacement in Z-direction was free and the displacements in X- and Y-directions were fixed. On the other hand, the tibial component was able to move freely in Y-direction and fixed in X- and Z-directions.

Load data used as the mechanical boundary condition was referred from the reference 2 in which load data for rapid deep squatting was analytically obtained using 2 dimensional model of human knee considering muscular forces. The load P1 and P2 were applied to the

femoral component in the vertical direction (Z-direction) and to the tibial component in the horizontal direction (Y-direction), respectively. The relationship between the load data and the flexion angle were shown with the body force used in the analysis in Fig.5.

A commercially available pre-processor FE-MAP was used to develop those 3D FEM models including solidification from the surface data, meshing and setting up of the boundary conditions. A commercial explicit finite element code LS-DYNA was then utilized as solver, and a post-processor LS-POST was used to analyze the FEM results.

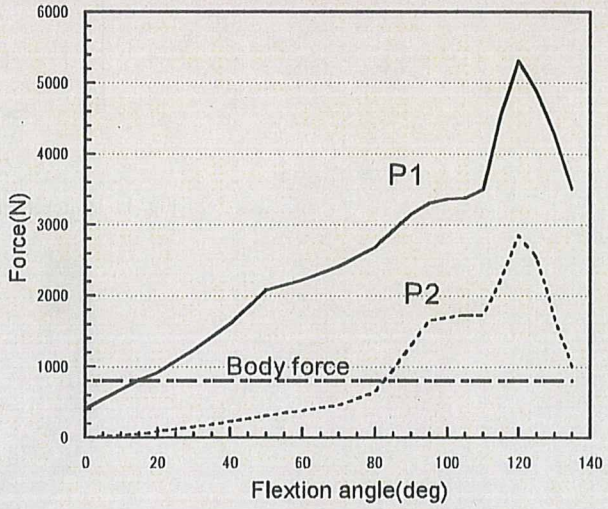

Fig. 5 Force-flexion angle relations used as mechanical boundary condition.

3. Results and Discussion

3.1 Mises equivalent stress distribution

Von Mises equivalent stress distributions of the tibial insert at 45 and 120 degrees of flexion are shown in Fig.6. At 45 degree, stress concentration occurred only on the condylar surfaces, and the maximum stress values of the 1st model and the 2nd model were 11.2 MPa and 17.6 MPa, respectively, indicating that the 2nd exhibited higher maximum stress than the 1st under the same boundary condition. The contact between Post and Cam did not take place at this angle. Larger stress concentration occurred on both the condylar and Post surfaces at 120 degree of flexion. The maximum stress values were 73.0 MPa for the 1st and 48.9 MPa for the 2nd, indicating that stress concentration was effectively reduced in the 2nd at deep flexion angle. It is also noted that the location of stress concentration on the condylar surfaces moved toward the back (Y-direction) as flexion proceeded from 45 to 120 degree, suggesting that roll-back movement was generated. The dependence of the displacement of the spring element on flexion angle is shown in Fig.7. The positive direction coincided with the negative Y-direction in Fig.4. There was no displacement generated up to about 60 degree and the displacement rapidly increased after 60 degree and the final displacement was approximately 12 mm. The difference between the two models was almost negligible. The displacement at the flexion angles greater than 60 degree corresponded to the displacement of the tibial component in the negative Y-direction, that is, so-called roll-back behavior in TKA.

Mises equivalent stress distributions in the cross-sectional areas of the tibial inserts at 120 degree of flexion are shown in Fig.8. It is clearly seen that the stress concentration region with the highest stress level of 40-50MPa was much wider in the 1st model than in the 2nd model. It is also interesting to see that for the 2nd, the highest stress concentration region was located inside of Post, suggesting that the possibility of delamination failure at this point.

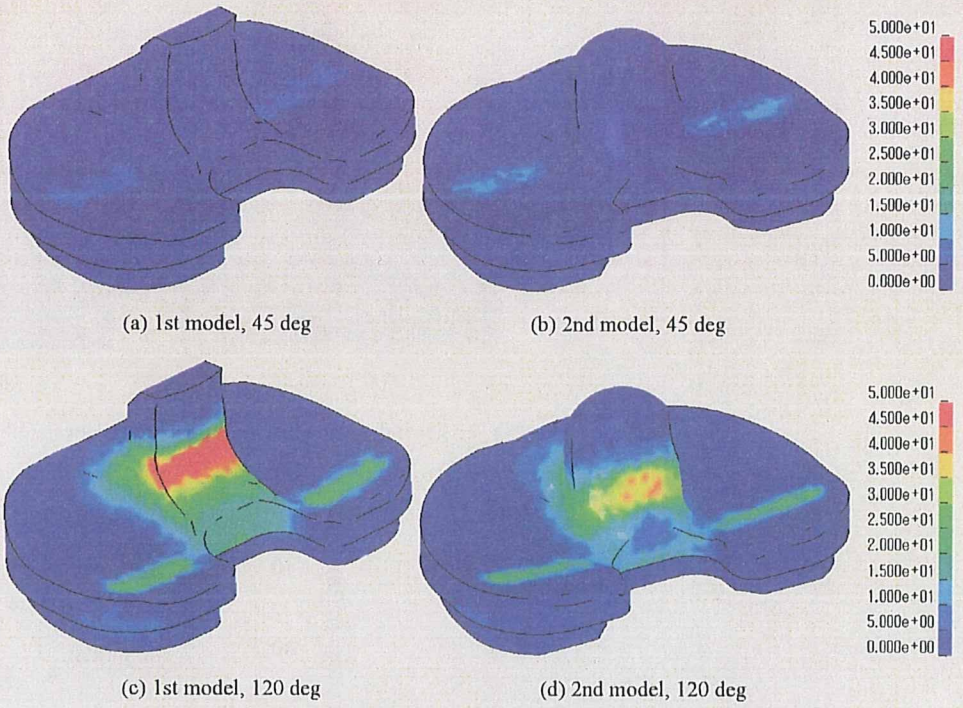

(a) 1st model, 45 deg (b) 2nd model, 45 deg

(c) 1st model, 120 deg (d) 2nd model, 120 deg

Fig. 6 Equivalent stress distribution on the surface of tibial insert (unit: MPa).

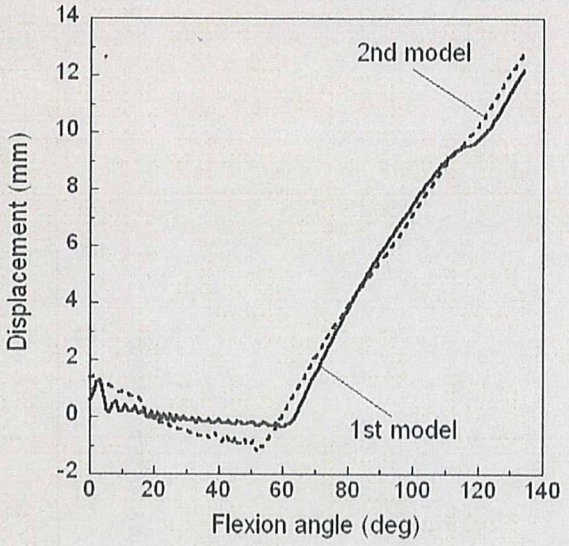

Fig. 7 Dependence of displacement of spring model on flexion angle.

3.2 Dependence of maximum equivalent stress on flexion angle

The dependences of the maximum equivalent stress values on flexion angle on the condylar surface and Post of the tibial inserts are shown in Fig.9. For the condylar surfaces, the maximum stress of the 2nd model was larger than that of the 1st model at flexion angles smaller than 60 degree. On the other hand, the 1st exhibited larger stress at angles greater than 120 degree, however the difference was not so large compared to the Post stress discussed later. The slope of the frontal condylar surface of the 2nd was designed to be a little gentler than that of the 1st; therefore, the contact area between the condylar surfaces of the femoral component and the tibial insert became smaller in the 2nd, resulting in the higher stress at angles smaller than 60 degree. The slope of the rear condylar surface of the 2nd was almost the same as that of the 1st and therefore, the difference of the stress became

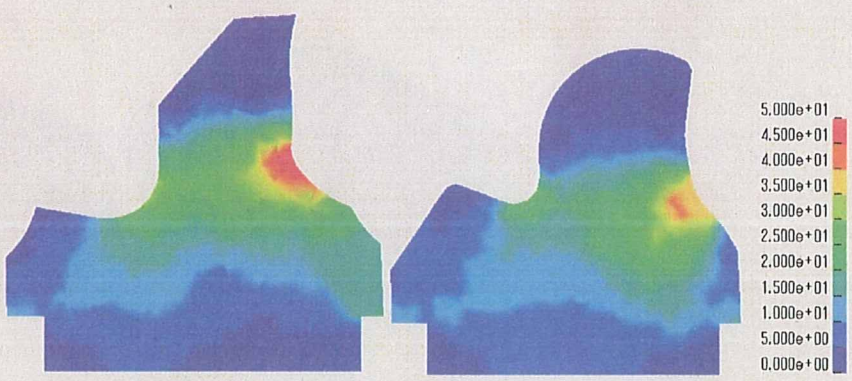

(a) 1st model (b) 2nd model

Fig. 8 Stress distribution in the cross-sectional area of tibial insert at 120 degree of flexion (unit: MPa).

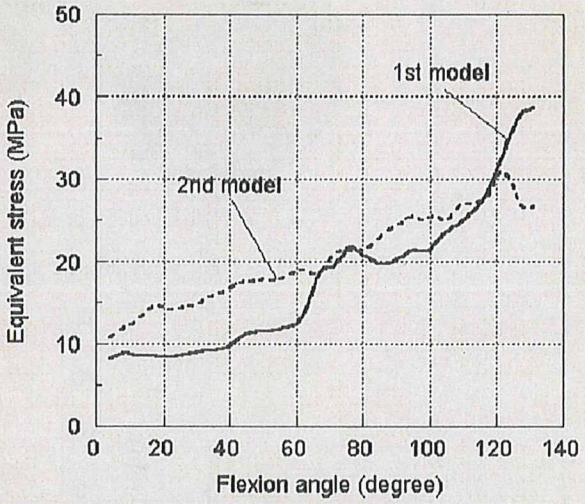

(a) condyle surface

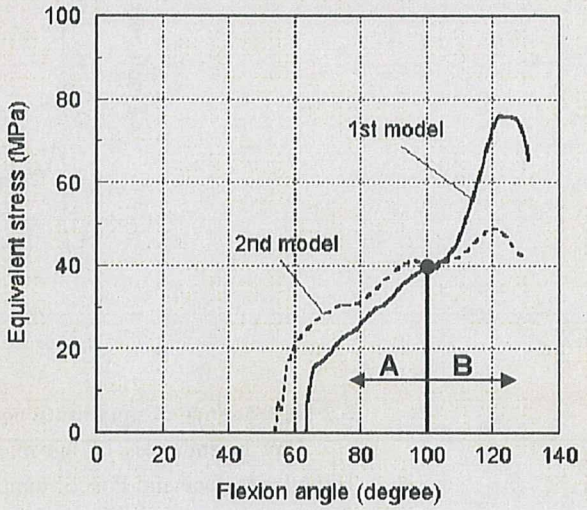

(b) Post surface

Fig. 9 Maximum equivalent stress history on the surface of tibial insert.

small. It was found that the contact between Post and Cam started at 64 degree in the 1st; on the contrary, the contact started at 54 degree in the 2nd. This difference was caused by the difference of the Post shape, i.e., Post of the 2nd was much larger than that of the 1st as a result of the shape modification. The Post surface stress of the 2nd was higher than that of the 1st up to 100 degree (region A in Fig.9(b)); on the contrary, at flexion angles greater

than 100 degree (region B), the 1st exhibited higher Post stress than the 2nd. The rapid increase of the Post stress of the 1st in region B is related to higher stress concentration due to smaller contact area between Post and Cam in the 1st than in the 2nd.

3.3 Effect of design modification on deep flexion motion

It was found from these analytical results discussed above that the design modification, especially Post and the surrounding region of Post, applied in the model change from the 1st model to the 2nd model effectively reduced stress concentration in Post and the surrounding region. This kind of reduction of stress concentration generally corresponds to reduction of the reaction force generated by the Post/Cam contact during deep flexion. Such reduction of the reaction force generally implies the decrease of resistance for deep flexion and therefore, the 2nd model is considered to be more suitable for deep flexion motion than the 1st model. In order to further confirm the superiority of the 2nd model, it is needed to analyze and compare the stress states under more complicated boundary conditions including flexion, rotation and lift-off.

4. Conclusions

3D FEM models of two different types of Stryker's PS type knee prostheses, the 1st model (Scorpio Superflex) and the 2nd model (Scorpio NRG), clinically used worldwide were constructed from their CAD data. Stress states of the two models were analyzed and compared under a condition of deep knee flexion by using the explicit finite element method. The conclusions are summarized as follows:

(1) A simplified 3D-FEA model of PS type knee prosthesis for deep knee flexion analysis was developed for the first time by using nonlinear spring model and load data for deep squatting. High stress concentration due to the Post-Cam contact was reasonably expressed at deep flexion angles and furthermore, roll-back behavior was well simulated by introducing the nonlinear spring model.

(2) Post surface stress of the 2nd model was higher than that of the 1st model up to 100 degree flexion; on the contrary, at flexion angles greater than 100 degree, the 1st model exhibited much higher Post stress than the 2nd model. This is due to higher stress concentration created by smaller contact area between Post and Cam in the 1st model than in the 2nd model.

(3) The modification of Post shape conducted in the designing process of the 2nd model effectively reduced the stress concentration at deep flexion angles. This kind of stress reduction is thought to correspond to the reduction of reaction force, indicating that the resistance to deep knee flexion is lower in the 2nd model than in the 1st model.

(4) The developed FEA model can easily be extended to express more complicated knee motions such as rotation and lift-off through modification of the boundary conditions. Further study on stress analysis under deep knee bending conditions using these models will give us some ideas towards new design concepts for knee prosthesis specially suiting to Japanese lifestyle.

References

(1) Ahir, S.P., Blunn, G.W., Haider H., Walker, P.S., Evaluation of a testing method for the fatigue performance of total knee tibial trays. Journal of Biomechanics, 32(1999), 1049-1057.

(2) Dahlkvis, N.J., Mayo, P., Seedhom, B.B., Forces during squatting and rising from a deep squat, Engineering in Medicine, 11(1982), 69-76.

(3) D'Lima, D.D., Chen, P.C., Kester, M.A., Colwell Jr, C.W., Impact of patellofemoral design on patellofemoral forces and polyethylene stresses, The Journal of Bone and Joint Surgery, 85A(2003), 85-93.

(4) Godest, A.C., Beaugonin, M., Haug, E., Taylor, M., Gregson, P.J., Simulation of a knee joint replacement during a gait cycle using explicit finite element analysis. Journal of Biomechanics, 35(2002), 267-275.

(5) Halloran, J.P., Anthony, J.P., Rullkoetter, P.J., Explicit finite element modeling of total knee replacement mechanics. Journal of Biomechanics, 38(2005), 323-331.

(6) Kanekasu, K., Scorpio Superflex total knee arthroplasty-Design, cilinical results and kinematics, Journal of Joint Surgery, 23(2004), 49-57.

(7) Kobayashi, K., Kakinoki, T., Tanabe, Y., and Sakamoto, M., Mechanical properties of ultra high molecular weight polyethylene under impact comporession - Property change with gamma irradiation and dynamic stress-strain analysis of artificial hip joint - , Journal of The Japanese Society for Experimental Mechanics, 3(2003), 225-229.

(8) Sathasivam, S., Walker, P.S., Computer model to predict subsurface damage in tibial inserts of total knees. Journal of Orthopaedic Research, 16(1998), 564-571.

(9) Morra, E.A., Greenwald, A.S., Polymer insert stress in total knee designs during high-flexion activities: a finite element study. Journal of Bone and Joint Surgery, Am 87(2005), 120-124.

(10) Todo, M., Nagamine, R., Kuwano, R., Hagihara, S., and Arakawa, K., Development of 3D finite element model of total knee arthroplasty and computational efficiency, Japanese Journal of Clinical Biomechanics, 27(2006), 231-237.

(11) Todo, M., Nagamine, R., Yamaguchi, S., Hagihara, S., and Arakawa, K., Effect of flexion and rotation on the stress state of UHMWPE insert in TKA, Japanese Journal of Clinical Biomechanics, 27(2006), 239-246.

(12) Watanabe, T., Yamazaki, T., Sugamoto, K., Tomita, T., Hashimoto, H., Maeda, D., Tamura, S., Ochi, T., and Yoshikawa, H., In vivo kinematics of mobile-bearing knee arthroplasty in deep knee bending motion, Journal of Orthopaedic Research, 22(2004), 1044-1049.

免疫

O-56

バナジウムの毒性とインターロイキン-6との関連性

Role of interleukin-6 on hepatic toxicity caused by vanadium compound in mice.

○長谷川達也[1]、小林一男[2]、佐藤雅彦[3]、姫野誠一郎[4]、瀬子義幸[1]

[1]山梨県環境科学研究所、[2]キッセイ薬品、[3]愛知学院大学、[4]徳島文理大学

【目的】我々はこれまでにバナジウムがメタロチオネイン（MT）を誘導合成すること、そして誘導合成されたMTにはバナジウムは結合しないことを明らかにしている。さらに、バナジウムによるMT誘導機構の一部にインターロイキン-6（IL-6）の関与することを報告した。今回、バナジウムの毒性とIL-6との関連性について検討を行った。

【方法】動物はICRマウス（5週齢、オス）、IL-6 nullマウス(9週齢、オス)および野生型マウス（B6J129Sv、9週齢、オス）を実験に用いた。メタバナジン酸アンモニウム(AMV)を0.05~0.3 mmol/kgの割合でマウスに皮下投与し、6あるいは24時間後に解剖し臓器を摘出した。臓器中MT量は水銀結合法で測定した。ASTならびにALT活性はドライケム測定装置で、IL-6はELISAキットでそれぞれ測定した。バナジウム量は臓器を硝酸-過酸化水素水で湿式灰化後、ICP-MSで測定した。

【結果・考察】ICRマウスにAMVを0.05～0.3 mmol/kg投与すると、バナジウムは主に腎臓に投与量依存的に蓄積した。肝臓にはわずかしかバナジウムは蓄積しなかった。しかし、MTは肝臓で有意に誘導合成された。IL-6 nullマウスおよび野生型マウスにAMVを投与した場合、肝臓中のMT量は、IL-6 nullマウスならびに野生型マウス共に増加したが、IL-6 nullマウスのMTは、野生型マウスの約50%であった。一方、血漿中ASTおよびALT活性を測定した結果、これら酵素活性は野生型マウスに比べIL-6 nullマウスの方が有意に高かった。これらの結果から、IL-6そのものかあるいはIL-6を介して誘導されたMTがバナジウムの毒性を軽減する可能性が考えられた。現在、MT nullマウスを用いてバナジウムの毒性軽減因子に関してさらに検討を行っている。

O-57

低濃度DBT曝露によるマクロファージ系細胞の生存率の低下、サイトカイン産生に対する影響

The effects of low-dose DBT on the viability and cytokine production of murine macrophage cell line, J774.1.

○ 角田正史[1]、吉田珠恵[2]、辻雅善[1,3]、張瑩[1,4]、菅谷ちえ美[1]、井上葉子[1]、三木猛生[1]、工藤雄一朗[1]、佐藤敏彦[1]、相澤好治[1]

Tsunoda, M., Yoshida, T., Tsuji, M., Zhang, Y., Sugaya, C., Inoue, Y., Miki, T., Kudo, Y., Satoh, T. and Aizawa, Y.

[1]北里大学医学部衛生学公衆衛生学、[2]北里大学医療衛生学部、[3]目白大学短期大学部、[4]国際医療福祉大学
[1]Kitasato University School of Medicine, Department of Preventive Medicine and Public Health, [2]Kitasato University School of Allied Health Sciences, [3]Mejiro University College, [4]International University of Health and Welfare

The effects of dibutyltin (DBT) on the cell viability and the productions of cytokines in a murine macrophage cell line, J774.1, were investigated. The mean value of the cell viability in the cells exposed to 0.125μM DBT was significantly lower than that in the controls. The mean concentration of tumor necrosis factor α (TNFα) or interleukin 12p40 (IL-12p40) in the supernatant of the activated cells exposed to DBT was significantly lower than the control, but not for the IL-10. It is suggested that DBT is toxic to macrophages, and the inhibition of the production of cytokines by DBT does not occur for all cytokines.

【目的】ジブチルスズ(DBT)化合物は安定剤や触媒として広く使用されている。我々は昨年、DBTによるマクロファージ系細胞、J774.1への影響として、生存率及び上清中の炎症性サイトカイン濃度の低下を報告した。今回はDBTについて、より低濃度の曝露も行い、有意な生存率の低下を示す閾値を探り、また、炎症性以外のサイトカインへの影響を明らかにすることを目的とした。

【方法】J774.1細胞を5% CO_2, 37℃の条件下で、5%のfetal bovine serumを含むRPMI1640培養液（抗生物質入り）で培養した。昨年の例を参考にDBT dichlorideを0, 0.5, 1.0, 1.5, 2.0 μMの濃度となるように曝露し、また0.5μM以下の、より低い濃度での曝露も行った。曝露後18時間の時点で、lipopolysaccharide (LPS)を最終濃度100ng/mlの濃度で添加した。更に24時間培養し上清を採取し、細胞の生存率をトリパンブルー色素排除法で検討した。上清中のtumor necrosis factor α (TNFα)、interleukin-10 (IL-10), IL-12のダイマーの一つであるIL-12p40の各濃度をELISAにて定量した。

【結果】細胞の生存率は、低濃度曝露を含めて検討した結果、0.125μMのレベルから対照群に比べて有意な低値を示した。上清中サイトカイン濃度に関しては、0-2.0 μMの曝露で、TNFα及びIL-12p40に関して全ての曝露群で対照群に比べて有意に低く、値自体も顕著に低かった。一方、IL-10に関しては1.5μM群で対照群及び他の群に比べて有意に平均値が高いという結果になった。

【考察】DBTのマクロファージに対する毒性は生存率の結果から判断すると、極めて強いことが示唆された。サイトカイン濃度に対しては、IL-12p40の低下から産生の抑制が起こるのは炎症性のサイトカインに限らないことと、また細胞死のみでは説明が出来ないことが示唆された。一方IL-10の結果から必ずしも全てのサイトカインで産生抑制が起きるのではないことが示唆された。

O-422

人工脳硬膜の安全性評価に関する研究（第2報）：人工硬膜埋め込みラットの行動学試験を用いた神経毒性評価

[1]北里大学 医学部 衛生学公衆衛生学、[2]目白大学 短期大学部、[3]神奈川県 環境農政部 県央家畜保健衛生所、[4]福嶋リハビリテーション学院、[5]北里大学 医療衛生学部 公衆衛生学、[6]同 生理学、[7]国立医薬品食品衛生研究所 療品部

○角田　正史[1]、辻　雅善[1,2]、木村　幸子[1,3]、張　瑩[1,4]、菅谷ちえみ[1]、井上　葉子[1]、工藤雄一朗[1]、佐藤　敏彦[1]、片桐　裕史[5]、秋田　久直[6]、佐治　眞理[6]、土屋　利江[7]、相澤　好治[1]

【目的】近年開発された脳外科用の合成生体吸収性人工硬膜は、乳酸ポリマー等の共重合体から成る。ポリマーの重合に触媒としてジブチルスズ（DBT）及びオクチル酸スズ（OT）が使われ、これらは人工硬膜に残存する。昨年の発表では、人工硬膜の神経毒性評価のためのモデル実験として、頭蓋骨を直径5㎜でくり抜き、人工硬膜またはDBTを高濃度含有する膜を埋め込み、4週後に脳各部位の神経伝達物質を測定し評価を行った。多くのラットで骨の再生が早く、膜が再生骨と戻した頭蓋骨の間にサンドイッチされてしまう、という問題があった。今回は頭蓋骨のくり抜きの直径をほぼ限界である1cmとし、control（手術のみを行う）群、人工硬膜製品埋め込み群、高濃度DBT（100ppm）含有ポリ乳酸ラクチド膜埋め込み群、高濃度OT（200ppm）含有ポリ乳酸ラクチド膜埋め込み群を設定し、オープンフィールド試験及びprepulse inhibition（PPI）testの行動学試験を用い評価することとした。以上より、吸収性人工硬膜の毒性評価法を確立するためのデータを得ることを目的とした。

【方法】雄のWistar系ラットをcontrol群、人工硬膜埋め込み群、高濃度DBT含有膜埋め込み群、高濃度OT含有膜埋め込み群の4群に分けた（n=10/群）。人工硬膜のオクチル酸スズの残存濃度は最大20ppmであった。高濃度DBT含有膜は残存スズの濃度を100ppm、高濃度OT含有膜は残存スズの濃度を200ppmとし作成した。ラットを脳定位固定装置に固定し、ドリルシステム及び内径1cmのボーントレフィンバーを用い頭蓋骨から直径1cmの円形の頭蓋骨片をくり抜いた。穴よりそれぞれの膜を頭蓋内に入れ、上から頭蓋骨片をかぶせた。手術後4週、同じ群から2匹ずつ一つのケージに入れ飼育した後、PPI testを行った。使用器械は小動物驚愕反応測定装　置、Startle Response System SR-LAB ABS systemであった。prepulseを80、75、70dBの大きさと（PP80、PP75、PP70）し、prepulseがない場合の驚愕反応測定値とある場合を比較しpercent prepulse inhibition（% PPI）をそれぞれのprepulse毎に計算した（% PPI at PP80、% PPI at PP75、% PPI at PP70）。

次いでオープンフィールド試験を行った。ラットを30分間動画で記録すると共に観察を行った。動画記録から行動距離を算出した。また観察により、各探索行動の回数等を記録し、最初に3秒以上のグルーミングを行った時点までの時間も測定した。オープンフィールド試験終了後、ラット脳を摘出し、膜を回収し、脳表面を観察した。

【結果】脳の観察では、膜が骨に挟まれている例は1例のみであったが、多くのラットで、脳表面に骨の切り出しに相当した痕があり、一部壊死している個体もあった。損傷が激しい例を除外し、control 8例、人工硬膜群5例、高濃度DBT含有膜群7例、高濃度OT含有膜群7例を行動学試験の解析対象とした。膜の吸収量の平均値±標準誤差は人工硬膜7.6 ± 2.1mg、高濃度DBT含有膜が7.6 ± 2.2mg、高濃度OT含有膜9.8 ± 1.9mgであった。PPI testの% PPI at PP80、% PPI at PP75、% PPI at PP7全てについて、群間で有意性を示さなかった。オープンフィールド試験の移動距離、群別の探索行動の回数、グルーミングの開始までの時間に関しても群間で有意差はなかった。

【考察】脳表面の損傷は大きく、頭蓋骨をくり抜く直径が大きすぎた可能性がある。直径には再検討の余地がある。骨に挟まれたのは1例のみで、膜の吸収も起こっていると考えられる結果であり、実際の手術に近い点もあった。今回の結果から本研究のプロトコール、評価方法に関する限り、人工硬膜の頭蓋内挿入により大きな生体影響はないことが示唆された。

P1－5

人工脳硬膜の安全性評価に関する研究：ポリ乳酸ラクチド膜埋め込みラットの神経伝達物質を用いた毒性評価

Evaluation of toxicity of poly (L-lactic acid-co-glycolic acid-co-caprolactone) containing dibutyltin or octyl acid tin in rats by neurotransmitters in brains

○角田正史[1]、辻　雅善[1,2]、木村幸子[1]、張　瑩[1,3]、菅谷ちえ美[1]、井上葉子[1]、
工藤雄一朗[1]、佐藤敏彦[1]、片桐裕史[4]、秋田久直[4]、佐治眞理[4]、土屋利江[5]、相澤好治[1]

○Masashi TSUNODA[1], Masayoshi TSUJI[1,2], Sachiko KIMURA[1], Ying ZHANG[1,3], Chiemi SUGAYA[1], Yoko INOUE[1], Yuichiro KUDO[1], Toshihiko SATOH[1], Hiroshi KATAGIRI[4], Hisanao AKITA[4], Makoto SAJI[4], Toshie TSUCHIYA[5], Yoshiharu AIZAWA[1]

[1]北里大学 医学部 衛生学公衆衛生学、[2]目白大学 短期大学部、[3]福島リハビリテーション学院、
[4]北里大学 医療衛生学部、[5]国立医薬品食品衛生研究所 療品部

[1]Preventive Medicine and Public Health, Kitasato University School of Medicine, Sagamihara, Japan [2]Mejiro Univ [3]Fukushima Rehabil [4]Kitasato Univ School Allied Health Sci [5]National Instit Health Sci

【背景】近年開発された脳外科用の合成生体吸収性人工硬膜は、ポリ（乳酸－グリコール酸－カプロラクトン等）共重合体（PLGC）で構成されている。重合に触媒としてジブチルスズ（DBT）及びオクチル酸スズ（OT）が使われ人工硬膜に残存する。今回、人工硬膜の毒性評価のためのモデル実験として、頭蓋骨くり抜きの直径をラットから考えほぼ最大である 1 cm とし、対照（手術のみを行う）群、人工硬膜（PLGC）の三層膜埋め込み群、高濃度 DBT 含有 PLGC 膜埋め込み群、高濃度 OT 含有 PLGC 膜埋め込み群を設定し、脳各部位の神経伝達物質の濃度を用い評価を行った。

【方法】雄のラットを対照群、PLGC 膜群（Sn＜20 ppm）、高濃度 DBT 含有 PLGC 膜群（Sn ＝ 100 ppm）、高濃度 OT 含有 PLGC 膜群（Sn ＝ 200 ppm）の 4 群に分けた（n ＝ 10/群）。ラットから内径 1 cm のボーントレフィンバーを用い直径 1 cm の円形の頭蓋骨片をくり抜き、穴よりそれぞれの膜を頭蓋内に入れた。手術の 4 週間後、ラット脳を大脳、小脳、延髄、中脳、線状体、下垂体に分割し、脳各部位より抽出したノルエピネフリン、ドーパミン及びセロトニン（5-HT）、それらの代謝産物を ECD 付き HPLC で測定した。

【結果】脳表面に骨切り出しに相当した痕があり、壊死がある個体もあった。損傷が激しい例を除外し、対照群 8 例、PLGC 膜群 5 例、高濃度 DBT 膜群 7 例、高濃度 OT 膜群 7 例で解析した。下垂体のドーパミン濃度が PLGC 群が他の群に比べて有意に高かった。小脳においては PLGC 膜群の 5-HIAA/5-HT の平均値が高濃度 OT 含有膜群に比べて有意に低かった。

【考察】脳の損傷は大きく、頭蓋骨をくり抜く直径が大きすぎた可能性があり、再検討の余地がある。ラットの死亡は起こらず実際の手術に近い点もあった。本研究のプロトコールに関する限り、PLGC 膜の頭蓋内挿入の生体影響は大きくはないことが示唆された。

Subtracted vortex centers path line method with cinematic angiography for measurement of flow speed in cerebral aneurysms

Makoto Ohta, Naoko Fujimura, Luca Augsburger, Krisztina Barath, Hasan Yilmaz, German Abdo, Karl-Olof Lovblad and Daniel A. Rüfenacht

Biofluid Control laboratory, Institute of Fluid Science, Tohoku University, Sendai 980-8577, Japan

Background and purpose: *The assessment of blood flow speed by imaging modalities is of increasing importance for endovascular treatment, such as stent implantation, of cerebral aneurysms. The subtracted vortex centers path line method (SVC method) utilizes image post-processing for determining flow quantitatively. In current practice, intra-aneurysmal flow in an* in vitro *model is visualized by laser sheet translumination and digitally recorded. In this study, we applied this method to cinematic angiography (CA), which is the preferred imaging method for endovascular interventions, to analyse hemodynamic changes. The SVC method was applied to the images and compared with results of the slipstream line method with colored fluid.*

Methods: *A transparent tubular model was constructed of silicone which included an aneurysm 10 mm in diameter and having a 5 mm neck on a straight parent artery with a diameter of 3.5 mm. The model was integrated into a pulsatile circulation system. By CA, successive images at 25 frames/s with injection of contrast were obtained.*

Results and conclusion: *Rotating vortexes of contrast, which advanced along the wall of the aneurysm, were observed in successive images of the aneurysm cavity. This phenomenon was also observed in the successive images with the slipstream line method. The speed of the vortex center was calculated and the results show that the vortex speed of CA was the same as that under the slipstream line method. This indicates the possibility of applying the SVC method to medical imaging equipment for analysis of the flow in aneurysms containing stent.* [Neurol Res 2007; **000**: 000–000]

Keywords: Subtracted vortex centers path line; cinematic angiography; stent; aneurysm; endovascular

INTRODUCTION

With the availability of flexible stent placement for intracranial aneurysms, this relatively new treatment is recently being increasingly utilized[1–4]. By decreasing the inflow into the aneurysm, stent treatment may lead to thrombus formation in intracranial aneurysms[5–10]. The stent design, e.g. the design of the stent edge, critically impacted on flow changes[11,12]. This is not the only stent parameter of interest and the influence of other important parameters such as porosity and filament diameter have been previously studied.

The assessment of blood flow by imaging modalities is of increasing importance. Magnetic resonance (MR), computed tomography (CT) and digital subtraction angiography (DSA) are the three major techniques currently being applied for this purpose.

Wakhloo *et al.* used Ethiodol droplets for measurement of flow in arteriovenous malformations[13]. Isoda *et al.*, for example, have investigated time-of-flight MR angiography in aneurysm models which enables the three-dimensional measurements[14]. To evaluate intra-aneurysmal hemodynamics using images acquired by DSA, Sadasivan *et al.*[15] and Asakura *et al.*[16] utilized time-density curves, and Sadasivan described the convection and diffusion components of flow and quantified the changes in flow in cerebral aneurysms after stents implantation.

The subtracted vortex centers path line (SVC) method was developed by Cassot and Barath, where an *in vitro* pulsatile circulation loop was seeded with particles and illuminated by a laser-sheet for measuring flow speed in a side-wall aneurysm model[17]. In this SVC method, post-processing of successive images is employed to trace a rotating vortex of particles from which the speed of the vortex movement in the aneurysm can be determined. This vortex speed represents intra-aneurysmal flow speed, which is a parameter that can be used for evaluating medical devices such as stents[18]. Although this processing is very simple and easily employed in the clinical field, it has only been used with *in vitro* setups, but never under *in vivo* conditions or by clinicians.

Correspondence and reprint requests to: Makoto Ohta, PhD, Biofluid Control laboratory, Institute of Fluid Science, Tohoku University, 2-1-1 Katahira, Aoba-ku, Sendai 980-8577, Japan. [ohta@biofluid.ifs.tohoku.ac.jp] Accepted for publication April 2007.

10.1179/016164107X230658

Neurological Research ner1271.3d 13/8/07 13:56:14
The Charlesworth Group, Wakefield +44(0)1924 369598 - Rev 7.51n/W (Jan 20 2003)

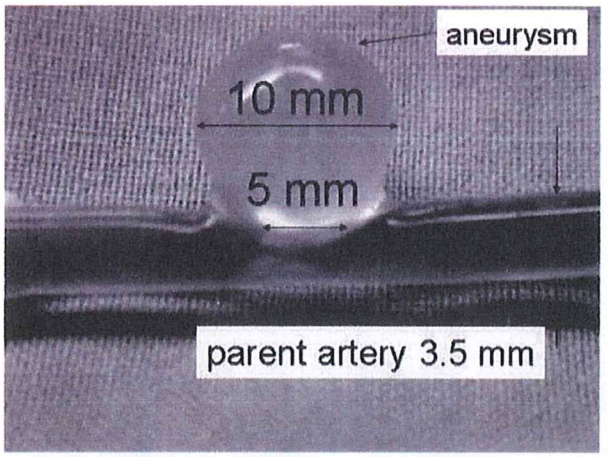

Figure 1: Transparent silicone model of an aneurysm with a 5 mm neck and a diameter of 10 mm on a straight parent artery with a diameter of 3.5 mm

In this study, the SVC method was applied to successive contrast images acquired with cinematic angiography (CA). The distance which a vortex moved was compared with a slipstream line acquired by video to validate and confirm the feasibility of integrating this method in medical imaging devices.

MATERIALS AND METHODS

In vitro model

A transparent tubular model made of silicone (Elastrat Sarl, Geneva, Switzerland) including an aneurysm with a 5 mm neck and a diameter of 10 mm, which was situated on a straight parent artery 3.5 mm in diameter (*Figure 1*), was integrated into a circulation system. The pressure and the pulsatility (143/77 mmHg and 1 Hz, respectively) were measured at the injection point in the system (the flowrate was 200 ml/min). Water was used as fluid at room temperature. For varying the flow pattern in the aneurysm, a stent (Leo stent, 4 mm diameter, 1.5 cm long; Balt, Montmorency, France) was prepared and the flow speeds before and after its placement were measured.

Image acquisition

CA

The image acquisition rate of CA (3D-RA, BV 3000; Philips Medical Systems, Best, The Netherlands) was 25 frames/s (fps) using imaging parameters of 60 kV and 300 mA. Each successive image was 512 × 512 bits in an 18.415 cm square with a 256 gray scale.

Slipstream line method

To compare images based on contrast with CA, a slipstream line was obtained by a video camera. Red hydrophilic liquid was introduced into the same circulation. The rate of the camera (DSC-T1; SONY, Tokyo, Japan) was 30 fps.

Post-processing

The SVC method was applied to the flow images of CA and the slipstream line, respectively, to quantify the flows.

All procedures of this processing were performed with commercially available based software packages which can be easily accessed by clinicians. Microsoft Photo Editor 3.01 (Microsoft Corporation, Redmond, WA, USA) was used for enhancement of image and subtraction was performed on Jasc Paint Shop Pro 6.00 (Jasc Software, Eden Prairie MN, USA). Tracing the vortex center was carried out with NIH images (Scion Corporation, Frederick, MD, USA).

RESULTS

Figure 2 shows successive images obtained from CA after stenting (top), as well as the enhanced images (middle). To extract the vortex movement, after the post-processing of two images, two images at successive times were subtracted one by one (bottom). The subtracted images exhibit the fluid entering the aneurysm with sufficient image contrast. The fluid in the aneurysm was composed of an inflow zone at the distal neck and an outflow zone at the proximal neck. A rotating vortex was formed in the distal zone of the aneurysm in each systole phase. The vortex circulated along the aneurysm wall rotating on itself. As the vortex traveled, it grew in diameter and lost its cohesion. The fluid in the aneurysm was pushed out in the diastole phase and at the beginning of the following systole phase. After enhancement of these images, two images of successive times were subtracted one by one to extract the vortex movement and then the center of the vortex was traced to measure the movement distance.

The slipstream line method was employed to compare and validate the images by contrast with CA. *Figure 3* shows successive enhanced images of the slipstream line indicating vortex movement. The inflow and outflow zones and the rotating direction of the vortex are the same as in the images from the CA with contrast.

Figure 4 shows a graph of movement distances depending on time of the vortexes without the stent after application of the SVC method. From *Figure 5*, which shows the distances with the stent, it can be seen that the contrast with CA corresponds with the slipstream line. *Figures 4* and *5* show that the speed of movement was reduced after stenting.

Table 1 shows the flow speeds after application of the SVC method from 0 to 0.4 seconds, respectively. The speed with CA was consistent with that with the slipstream line. The speed was reduced after stent placement.

DISCUSSION

Flow speed in the aneurysm cavity is one of the most important parameters to evaluate circulation of the blood in a cerebral aneurysm, shear stress and the functioning of medical devices.

Neurological Research ner1271.3d 13/8/07 13:56:34
The Charlesworth Group, Wakefield +44(0)1924 369598 - Rev 7.51n/W (Jan 20 2003)

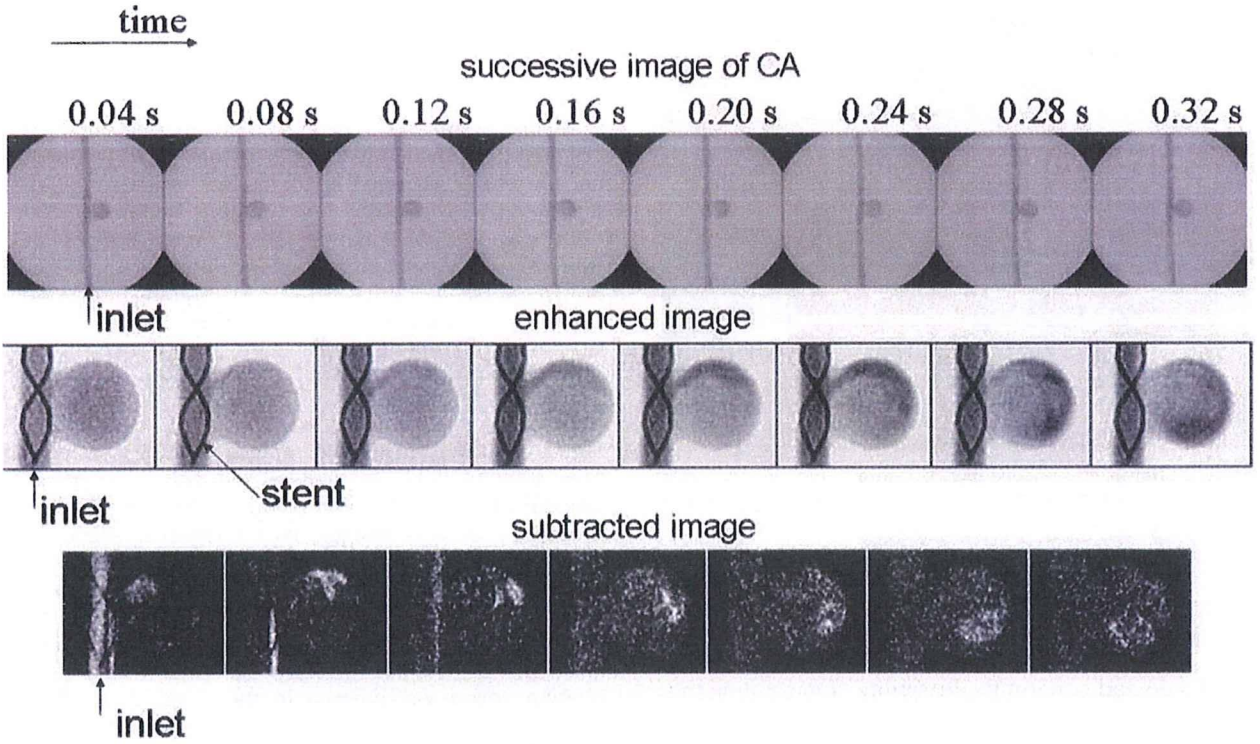

Figure 2: Successive images obtained from CA and the post-processing of the images. The top shows raw images, the middle presents enhanced images and the bottom shows subtracted images

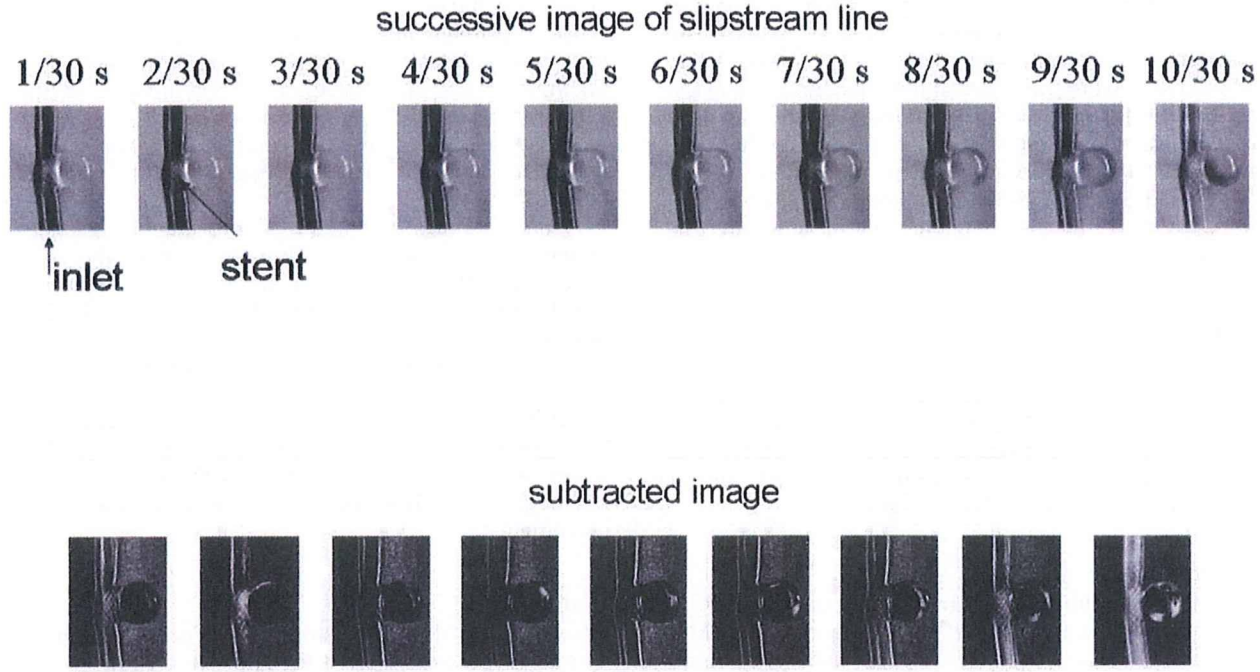

Figure 3: Successive images obtained from a slipstream line and the post-processing of the images. The top shows raw images and the bottom presents subtracted images

Neurological Research ner1271.3d 13/8/07 13:56:38
The Charlesworth Group, Wakefield +44(0)1924 369598 - Rev 7.51n/W (Jan 20 2003)

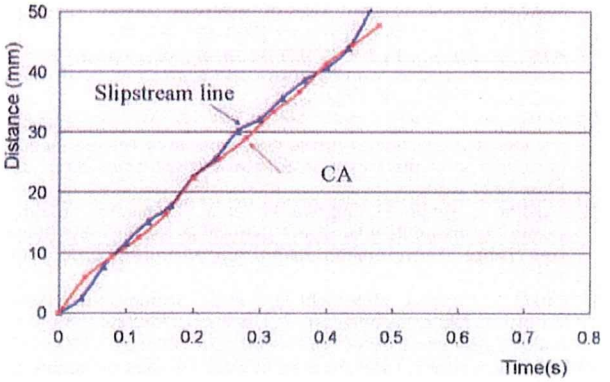

Figure 4: Graph of movement distances depending on time of the vortexes without the stent application of the SVC method for comparison between CA and slipstream line

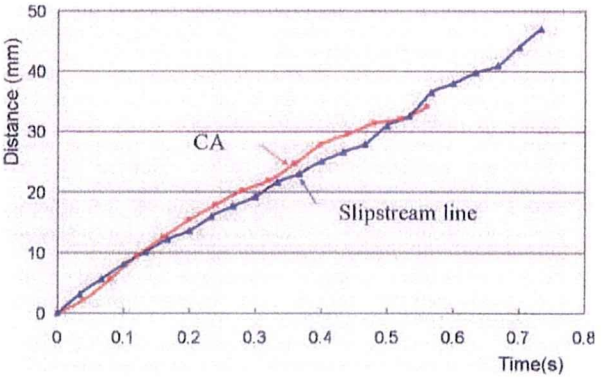

Figure 5: Graph of movement distances depending on time of the vortexes with the stent after application of the SVC method for comparison between CA and slipstream line. The flow speeds are reduced after the stenting when compared with *Figure 4*

The integration of the SVC method into medical imaging devices may allow not only medical engineers but also all clinical operators to use this method for analysis of the flow in aneurysms and evaluation of the influence of medical devices on blood speed. The results of contrast movements were consistent with those of the slipstream line, indicating the possibility of using the SVC method in the medical field.

The SVC we employed in our study consisted of several free or relatively inexpensive software packages, which suggests that many operators or technicians can easily adopt this system.

The contrast image was performed by CA, which is capable of imaging 25 fps. When compared with conventional frames per second such as 2 or 6 fps, CA can trace the vortex more smoothly and accurately[15].

The reduction in speed of vortex movement after stent placement in the aneurysm was consistent with many previous results[7,8,12,17,19]. Such reduction may lead to formation of a thrombus and allow repair of the aneurysm by occlusion.

Several drawbacks of application of the SVC method to medical images should be mentioned.

The tubular model, which was simplified with one straight parent artery and one simple aneurysm in this study, may induce a different flow pattern from that of a realistic model or that of an actual patient. However, because Barath performed the SVC method with a realistic model and the employed particles exhibited a rotating vortex along the aneurysm[17], it should be possible to apply and carry out this method with CA in a realistic model or patient if the vortex is detected.

The tubular model made of silicone may limit lateral displacements of the wall with the pulsatile flow because silicone has a lower compliance than a real vessel. The wall displacements may be larger when used with the Poly(vinyl alcohol) model developed by Ohta *et al.*[20] and may change the flow pattern.

Nitinol used for a self-expandable stent is hard to visualize with angiography, and with stent markers, only the position of a stent can be detected. Although the Leo stent (Balt, Montmorency, France) with highly radiopaque wires allowed greater visibility in this study, the structure near the neck was invisible compared with the case of a coronary stainless steel stent[21].

The spatial resolution of DSA should be improved if contrast images are to be used as way of measuring flow speed. The resolution in this study was 0.36 mm/pixel and so there were only ~28 pixels on the diameter of aneurysm. Micro-angiography may provide a good view around the neck of an aneurysm in perforated vessels[22].

Table 1: List of flow speeds after application of the SVC method from 0 to 0.4 seconds

	Without stent	With stent
Slipstream line (mm/s)	106.8 ± 11.3	72.3 ± 10.1
CA (mm/s)	109.6 ± 13.7	70.9 ± 7.7

CONCLUSION

To measure the blood flow speed in a cerebral aneurysm using DSA, the SVC method was applied to successive images of CA. The obtained successive images were clear, indicating the possibility of its use for evaluating the impact of stents on flow speed in cerebral aneurysms. The rotating vortex along the aneurismal wall was observed and its movement was consistent with the images of the slipstream line.

ACKNOWLEDGEMENTS

We are thankful to Mr J. Thyregod (COOK-WCE) and Mr D. Babic (Philips Medical Systems) for financial grants, Philips Medical Systems for mechanical techniques, Dr F. Betting for facilitating access to data in Geneva University Hospital, and Dr F. Cassot (INSERN, Toulouse, France) for his pioneering development of the SVC method

REFERENCES

1 Fiorella D, Albuquerque FC, Han P, *et al.* Preliminary experience using the Neuroform stent for the treatment of cerebral aneurysms. *Neurosurgery* 2004; **54**: 6–16

2 Howington JU, Hanel RA, Harrigan MR, *et al.* The Neuroform stent, the first microcatheter-delivered stent for use in the intracranial circulation. *Neurosurgery* 2004; **54**: 2–5

3 Lopes D, Sani S. Histological postmortem study of an internal carotid artery aneurysm treated with the Neuroform stent. *Neurosurgery* 2005; **56**: E416
4 Lylyk P, Ferrario A, Pasbon B, *et al.* Buenos Aires experience with the Neuroform self-expanding stent for the treatment of intracranial aneurysms. *J Neurosurg* 2005; **102**: 235–241
5 Lieber BB, Livescu V, Hopkins LN, *et al.* Particle image velocimetry assessment of stent design influence on intra-aneurysmal flow. *Ann Biomed Eng* 2002; **30**: 768–777
6 Rhee K, Han MH, Cha SH. Changes of flow characteristics by stenting in aneurysm models: Influence of aneurysm geometry and stent porosity. *Ann Biomed Eng* 2002; **30**: 894–904
7 Steiger HJ, Perktold K. Computer modeling of intracranial saccular and lateral aneurysms for the study of their hemodynamics. *Neurosurgery* 1997; **41**: 326–327
8 Aenis M, Stancampiano AP, Wakhloo AK, *et al.* Modeling of flow in a straight stented and nonstented side wall aneurysm model. *J Biomech Eng* 1997; **119**: 206–212
9 Hirabayashi M, Ohta M, Rufenacht DA, *et al.* Characterization of flow reduction properties in an aneurysm due to a stent. *Phys Rev E Stat Nonlin Soft Matter Phys* 2003; **68**: 021918
10 Hirabayashi M, Ohta M, Rufenacht DA, *et al.* A lattice Boltzmann study of blood flow in stented aneurysms. *FGCS* 2003; **20**: 925–934
11 Hamuro M, Palmaz JC, Sprague EA, *et al.* Influence of stent edge angle on endothelialization in an *in vitro* model. *J Vasc Interv Radiol* 2001; **12**: 607–611
12 Ohta M, Hirabayashi M, Wetzel S, *et al.* Impact of stent design on intra-aneurysmal flow: A computer simulation study. *Interv Neuroradiol* 2004; **10**: 85–94
13 Wakhloo AK, Lieber BB, Rudin S, *et al.* A novel approach to flow quantification in brain arteriovenous malformations prior to enbucrilate embolization: Use of insoluble contrast (Ethiodol droplet) angiography. *J Neurosurg* 1998; **89**: 395–404
14 Isoda H, Ramsey RG, Takehara Y, *et al.* MR angiography of aneurysm models of various shapes and neck sizes. *AJNR Am J Neuroradiol* 1997; **18**: 1463–1472
15 Sadasivan C, Lieber BB, Gounis MJ, *et al.* Angiographic quantification of contrast medium washout from cerebral aneurysms after stent placement. *AJNR Am J Neuroradiol* 2002; **23**: 1214–1221
16 Asakura F, Tenjin H, Sugawa N, *et al.* Evaluation of intra-aneurysmal blood flow by digital subtraction angiography: Blood flow change after coil embolization. *Surg Neurol* 2003; **59**: 310–319
17 Barath K, Cassot F, Rufenacht DA, *et al.* Anatomically shaped internal carotid artery aneurysm *in vitro* model for flow analysis to evaluate stent effect. *AJNR Am J Neuroradiol* 2004; **25**: 1750–1759
18 Barath K, Cassot F, Fasel JH, *et al.* Influence of stent properties on the alteration of cerebral intra-aneurysmal haemodynamics: Flow quantification in elastic sidewall aneurysm models. *Neurol Res* 2005; **27** (Suppl. 1): S120–S128
19 Yu SC, Zhao JB. A steady flow analysis on the stented and non-stented sidewall aneurysm models. *Med Eng Phys* 1999; **21**: 133–141
20 Ohta M, Handa A, Iwata H, *et al.* Poly-vinyl alcohol hydrogel vascular models for *in vitro* aneurysm simulations: The key to low friction surfaces. *Technol Health Care* 2004; **12**: 225–233
21 Rudin S, Wu Y, Kyprianou I, *et al.* Micro-angiographic detector with fluoroscopic capability. *Proc. SPIE* 2002; **4682**: 344–354
22 Rudin S, Wang Z, Kyprianou I, *et al.* Measurement of flow modification in phantom aneurysm model: Comparison of coils and a longitudinally and axially asymmetric stent – initial findings. *Radiology* 2004; **231**: 272–276

Neurological Research ner1271.3d 13/8/07 13:57:28
The Charlesworth Group, Wakefield +44(0)1924 369598 - Rev 7.51n/W (Jan 20 2003)

総　説

脳血管内カテーテル／ガイドワイヤシミュレータの開発

高嶋一登*，大田慎三**，太田　信***
葭仲　潔****，向井利春*

Development of a catheter and guidewire simulator for interventional therapy

Kazuto TAKASHIMA* Shinzo OTA** Makoto OHTA***
Kiyoshi YOSHINAKA* and Toshiharu MUKAI*

*Bio-Mimetic Control Research Center, RIKEN,
2271-130 Anagahora, Shimoshidami, Moriyama-ku, Nagoya, Aichi, 463-0003, Japan
**Oota Memorial Hospital,
3-6-28 Okinogami, Fukuyama, Hiroshima, 720-0825, Japan
***Institute of Fluid Science, Tohoku University,
2-1-1 Katahira, Aoba-ku, Sendai, Miyagi, 980-8577, Japan
****Department of Bioengineering, The University of Tokyo,
7-3-1, Hongo, Bunkyo-ku, Tokyo, 113-8656, Japan
[Received: 6 February 2008]

We have developed a catheter and guidewire simulator for interventional therapy. This system was developed to predict the course of approach to a lesion and to present numerical results and animation for surgical planning, intra-operative assistance, the analysis of the structure of the guidewire and the design of a new guidewire. The model of the guidewire is constructed with viscoelastic springs and segments as the dynamic deformation of a flexible structure. The proximal part of the guidewire is inserted into the catheter model. The vessel is an elastic circular cylinder whose shape is defined by the centerline and the radii. Collisions between the guidewire and the vessel are calculated and the contact forces are determined according to the stiffness and friction of the vessel wall. In this article, we introduce our simulator and several examples of the simulation results.

Key Words: Interventional therapy, Computer assisted therapy planning, Simulation, Catheter, Guidewire

＊理化学研究所　バイオ・ミメティックコントロール研究センター［〒463-0003　愛知県名古屋市守山区下志段味穴ヶ洞2271-130］
＊＊大田記念病院　〒720-0825　広島県福山市沖野上町一丁目6－28］
＊＊＊北大学 流体科学研究所［〒980-8577　仙台市青葉区片平2-1-1］
＊＊＊＊東京大学大学院　工学系研究科　〒113-8656　東京都文京区本郷7-3-1

1. はじめに

脳動脈瘤は破裂時の致死率が高いが，未破裂の状態では症状も少ない上に，破裂しない場合もある．そのため，脳動脈瘤の破裂を未然に防ぐ手術を行なう場合，破裂の可能性と手術に伴うリスクを考慮に入れて検討する必要がある．脳動脈瘤や脳梗塞の治療のために，細長い管状のカテーテル/ガイドワイヤ（頭部用マイクロガイドワイヤーで1.8－2 m，直径1 mm以下）を大腿部内側から血管を経て頭部にアプローチし，瘤内腔をコイルで塞栓したり，狭窄血管をバルーンで拡張したりする低侵襲治療法が盛んに行われている．この手法は開頭切開を伴わないため身体に負担の少ない治療方法であるが，体外から押し/引きとねじりのみで非常に細長い管を複雑な屈曲・分岐の多い血管内に挿入するので熟練した医師の高度な技術を必要とする．また，疾患によっては血管壁自体が弱くなっているので，ガイドワイヤによる穿孔の危険もある．

そのような血管内治療の安全性向上のために，国内外で，血管・カテーテル等の力学特性をパラメータに持つ方程式をコンピュータ上で解くさまざまなカテーテル挿入シミュレータが開発されている[1-10]．これらは，血管，カテーテル等の力学特性・形状や挿入手技によるパラメータを持つシミュレータをコンピュータ上に構築し，シミュレーションを行なっている．しかし，これらは力覚インターフェースを介しての挿入手技に対するカテーテルの動きをシミュレートし，挿入感覚をフィードバックするトレーニング用のものが多い．

それに対し，我々はこれまで術前・術中におけるカテーテル経路予測用シミュレータを開発してきた[11,12]．本システムは，PC上でターゲットである患部に対して，カテーテルがアプローチする経路を計算し，結果を数値データと動画で表示する．患部への経路が推定できることにより，術者は術前計画で，血管内治療の開頭クリッピング術に対する優位性や手術手順の検討，ガイドワイヤの種類（先端の曲げ角度，柔らかさ等）等を絞り込むことができる．また，術中でもX線透視像上の実際のカテーテル走行経路とシミュレーション結果との比較により，迅速な手術が支援できる．さらに，動画の視覚的，直感的な特徴を生かし，患者にとっては理解しやすく，医師にとっては説明が行ないやすい患者個別のコミュニケーションツールを提供することが可能である．本稿では，我々が開発してきたカテーテル経路予測用シミュレータの解析方法，および，これまで得られた主な結果について紹介する．

2. 解析方法

2.1 ガイドワイヤモデル

本研究では，急な手術でも術前計画に用いることができるように，高精度な解は得られるが計算時間を要する有限要素法を用いた解析は用いなかった．解析モデルの一例をFig. 1に示す（本モデルを用いた計算結果は3章に示す）．ガイドワイヤは，n個の円筒形の剛体セグメントが弾性バネと粘性ダッシュポットで直列結合した多関節リンクと仮定した．無負荷のセグメント長を，両端で$L_i/2$，それ以外でL_iとした．仮想ばねの両端の点に$n+1$個の節点を配し，術者側から順次節点番号を付けた．部材の伸縮変形は無視し，曲げ・ねじり変形は，根元の第1関節から第$n-1$関節にそれぞれ3自由度の回転機構を与え，その関節の粘弾性にて記述した．その粘弾性により，節点を挟んで前後$L_i/2$部分の曲げ・ねじり剛性をあらわした．個々のセグメントの運動は並進と回転を考え，各セグメントの接触時の接触力$\boldsymbol{F}_i$を求め，Newton-Euler運動方程式を用いて次式のように定式化した．

$$\boldsymbol{M}(\boldsymbol{q})\ddot{\boldsymbol{q}}+\boldsymbol{V}(\boldsymbol{q},\dot{\boldsymbol{q}})=\sum_{i}^{n}\boldsymbol{J}_i^T(\boldsymbol{q})\boldsymbol{F}_i+\boldsymbol{T} \quad (1)$$

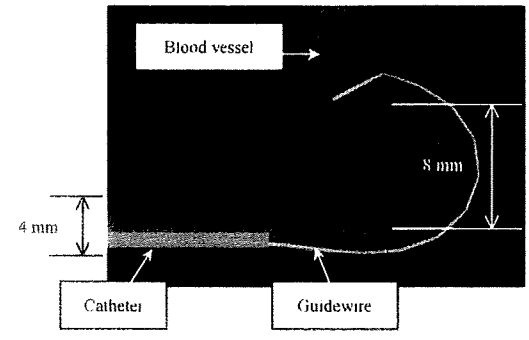

Fig. 1 Simulation models of guidewire, catheter and blood vessel.

$$T = -K_c(q - q_o) - D_c\dot{q} \quad (2)$$

ただし，qは関節変位ベクトル，q_oは仮想弾性ばねが自然長のときの関節変位ベクトル，Mは慣性行列，Vは遠心力・コリオリ力を表す速度項，Tは関節の粘弾性により生じるトルク，K_c，D_cはそれぞれ各関節の弾性係数，粘性係数である．また，Kcは，曲げ変形K_{cv}，ねじり変形K_{cc}に関してそれぞれ独立に，

$$K_{cv} = E_c I_v / L_c \quad (3)$$

$$K_{cc} = G_c I_p / L_c \quad (4)$$

で近似した[13), 14)]．ただし，E_c，G_cはそれぞれガイドワイヤの縦弾性係数，横弾性係数，I_v，I_pはそれぞれ断面二次モーメント，断面二次極モーメントである．本研究では，半径R_cの丸棒であるので，K_{cv}，I_pは以下の式になる．

$$K_{cv} = \pi E_c R_c^4 / 4L \quad (5)$$

$$I_p = 2 I_v \quad (6)$$

等方性材料と仮定すると，ポアソン比νを用いて，

$$G_c = E_c / 2(1 + \nu) \quad (7)$$

である．

2.2 血管モデル

血管は内径が均一な弾性円筒と仮定した．本研究では，血管の中心曲線を数値データで与え，その各中心点を中心とする半径Rvの円筒を設定することで，血管モデルを形成した．ただし，その中心線をあらわす$m \times 3$行列データ$s = [s_1^T \ s_2^T \ s_3^T \ \cdots \ s_m^T]^T$とした（$s_i$は各中心点をあらわす位置ベクトルである）．また，血管の内壁はそれぞれの初期位置との間に血管の半径方向に弾性（弾性係数K_v），接線方向に摩擦抵抗（血管とガイドワイヤ間の摩擦係数μ）を持つモデルとした．ただし，血管の変形を簡単化するために，血管の変形は内壁の変形のみで中心線は変位しないと仮定した．

2.3 接触反力の算出

ガイドワイヤが受ける反力の算出は，以下の手順で行なった．

1．ガイドワイヤが血管を押し込んだ方向ベクトルl_i（$= p_i - s_k$：p_iはガイドワイヤモデルの各関節および先端の位置ベクトル，s_kは血管モデルの中心線データsの中でp_iと最小距離をとる中心点）を求め，$|l_i| + R_c \geqq R_v$の場合，ガイドワイヤと血管は接触をしているものとする．このとき血管の中心線に垂直な方向に働く接触力f_{ni}は以下の式であらわされる．

$$f_{ni} = -K_v(|l_i| + R_c - R_v)^{3/2} l_i / |l_i| \quad (8)$$

2．その点での血管の中心線に接する方向の単位ベクトルu_{ti}を以下の式で求める．

$$u_{ti} = (s_{k+1} - s_k) / |s_{k+1} - s_k| \quad (9)$$

摩擦係数μを用い，血管の中心線に接する方向の摩擦力f_{ti}を以下の式で求める．

$$f_{ti} = -\mu |f_{ni}| u_{ti} \, \mathrm{sign}(u_{ti} \cdot \dot{q}) \quad (10)$$

ただし，sign (x) は次式で定義される符号関数である．

$$\mathrm{sign}(x) = \{1 \ (x > 0)\}, \{0 \ (x = 0)\}, \{-1 \ (x < 0)\} \quad (11)$$

さらに血管円形断面の円周方向の単位ベクトルu_{ci}を以下の式で求める．

$$u_{ci} = (u_{ti} \times l_i) / |u_{ti} \times l_i| \quad (12)$$

その方向についての摩擦力f_{ci}も，式(10)と同様に以下の式で求める．

$$f_{ci} = -\mu |f_{ni}| u_{ci} \, \mathrm{sign}(u_{ci} \cdot \dot{q}) \quad (13)$$

式(8)，(10)，(13)より，接触力を以下の式であらわす

$$F = f_{ni} + f_{ti} + f_{ci} \quad (14)$$